

# Machine-learned nodal structures of Fermion systems

William Freitas,<sup>1</sup> B. Abreu,<sup>2</sup> and S. A. Vitiello<sup>1</sup>

<sup>1</sup>*Gleb Wataghin Institute of Physics, University of Campinas (UNICAMP), 13083-970 Campinas, SP, Brazil*

<sup>2</sup>*Pittsburgh Supercomputing Center, Carnegie Mellon University, Pittsburgh, PA 15213, USA*

A major challenge in quantum physics is the accurate simulation of fermionic systems, particularly those involving strong correlations. While effective for bosonic systems, traditional quantum Monte Carlo methods encounter the notorious sign problem when applied to Fermions, often resulting in biased outcomes through the fixed-node approximation. This work demonstrates the potential of machine learning techniques to address these limitations by allowing nodal structures to be learned through gradient descent optimization iterations and the variational algorithm. Using a neural network to represent the wave function, we focus on quantum dots containing up to 30 electrons. The results show a significant reduction in the variational bias, achieving greater accuracy and a lower ground state energy than diffusion Monte Carlo with the fixed-node approximation. Our approach paves the way for precise and accurate property predictions in fermionic strongly correlated systems, advancing fundamental understanding and applications in quantum technologies.

*Introduction* - From quantum chromodynamics and nuclear matter to ultracold gases, liquid helium, and electrons in solids, mean-field or perturbation theories are often insufficient to describe observed physical phenomena in systems composed of strongly correlated Fermions [1–5]. In these cases, describing these correlations accurately and precisely is critical to achieving correct predictions. Despite the diversity of these systems, they are amenable to a standard set of tools from quantum Monte Carlo (QMC) methods rooted in non-relativistic quantum mechanics [6].

Quantum dots (QD), a relevant system with potential quantum devices applications for quantum computation and information storage [7–9], have been an active research platform, experimentally and theoretically [10, 11], with recent impactful developments, especially as QD arrays emerge as promising platforms for exploring excitonic states of matter [12]. These arrays can potentially be applied in scalable quantum computing and other quantum technologies [13–18]. Additionally, these quantum systems can realize generalized Fermi-Hubbard physics, providing a rich environment for advancing condensed matter physics and our understanding of quantum many-body systems [19, 20].

In QMC, when sampling the antisymmetric wave function of fermionic systems, cancellations between positive and negative contributions can make computations of expected values intractable even for the simplest observables, which is widely known as the sign problem [21, 22]. The fixed-node approximation, which constrains random walks to regions where the many-body wave function retains a single sign, is a popular way to mitigate this problem and has yielded generally good results for various systems [23–26]. However, it introduces an intrinsic bias since the nodal structure used in the approximation is an *a priori* component that can be arbitrarily chosen.

Machine learning (ML) is a promising approach to finding effective many-body wave functions of these systems because it allows us to explore functional forms

beyond traditional trial functions used in QMC methods [27]. Deep neural networks (DNNs) can represent highly nontrivial wave functions, offering a more flexible and potentially more powerful system description [28, 29]. This flexibility leads to better approximations of the true nodal structure, ultimately improving the accuracy of QMC simulations while directly attenuating the bias introduced by fixed-node approaches.

In this work, we demonstrate the potential of ML techniques to overcome a longstanding challenge by allowing the nodal structure to be learned during the optimization process guided by the variation algorithm. We focus on QD systems containing up to 30 electrons and show that the variational bias introduced by QMC methods can be significantly reduced or even eliminated by representing the many-body wave function through a neural network (NN). This leads to statistically better results for the system’s ground state energy than those obtained via the diffusion Monte Carlo method using the fixed-node approximation. In addition, these NN representations can be efficiently computed using graphical process units (GPUs), and their derivatives can be calculated without uncertainty from numerical errors using automatic differentiation.

*Methods* - We investigate a system of circular QDs made from semiconductor heterostructures, which is modeled by electrons interacting via the Coulomb potential and confined within a two-dimensional harmonic trap. With  $N$  electrons placed in the  $z = 0$  plane, this model’s Hamiltonian is

$$\mathcal{H} = \frac{-\hbar^2}{2m^*} \sum_i^N \nabla_i^2 + \frac{m^* \omega^2}{2} \sum_i^N (r_i^\alpha)^2 + \frac{e^2}{\varepsilon} \sum_{i < j} \frac{1}{r_{ij}}, \quad (1)$$

where  $m^*$  is the effective mass the electron,  $\hbar$  is the reduced Planck constant,  $\omega$  is the angular frequency of the harmonic trap,  $\varepsilon$  is the dielectric constant of the semiconductor,  $e$  is the electron charge and  $r_{ij} = |\mathbf{r}_i^\alpha - \mathbf{r}_j^\alpha|$

is relative distance between electrons  $i$  and  $j$  with spins  $\alpha$  and  $\alpha'$ , respectively, where  $\alpha$  and  $\alpha'$  can be either spin up ( $\uparrow$ ) or down ( $\downarrow$ ).

In practice, we employ a dimensionless Hamiltonian form  $\hat{\mathcal{H}}$  by introducing the effective Hartree  $E_{\text{H}}^* = \hbar^2/m^*(a_{\text{B}}^*)^2$  as the energy scale, where  $a_{\text{B}}^*$  the effective Bohr radius,  $a_{\text{B}}^* = \varepsilon\hbar^2/k_e m^* e^2$  and  $k_e$  is the Coulomb constant. With  $\lambda = E_{\text{H}}^*/\hbar\omega$  dictating the relative importance of the confining potential and the Coulomb interaction, this form is

$$\hat{\mathcal{H}} = -\frac{1}{2} \sum_i^N \hat{\nabla}_i^2 + \frac{1}{2\lambda^2} \sum_i^N (\hat{r}_i^\alpha)^2 + \sum_{i<j} \frac{1}{\hat{r}_{ij}}, \quad (2)$$

where  $\hat{r}_i^\alpha = r_i^\alpha/a_{\text{B}}^*$ .

We choose parameters based on a quantum dot of gallium arsenide, GaAs, which has an electronic effective mass  $m^* = 0.067m_e$  ( $m_e$  is the electron mass), and a dielectric constant  $\varepsilon = 12.7$  [30]. For the confining trap, we chose  $\hbar\omega = 0.28E_{\text{H}}^*$ , a typical value in the literature investigating the behavior of quantum dots [31].

To represent the wave function of this fermionic system, we cast a neural network representation based on the FermiNet approach [32–34], which allows for flexible representation of complex wave functions, and use this form to conduct QMC variational simulations coupled to optimization steps iteratively. The trial wave function  $\psi(\mathbf{r}_1^\uparrow, \dots, \mathbf{r}_{N/2}^\uparrow, \dots, \mathbf{r}_N^\downarrow)$  is expressed as:

$$\psi(\mathbf{r}_1^\uparrow, \dots, \mathbf{r}_{n^\downarrow}^\downarrow) = \sum_k \omega_k \det \left[ \phi_i^{k\uparrow}(\mathbf{r}_j^\uparrow; \{\mathbf{r}_{/j}^\uparrow\}; \{\mathbf{r}^\downarrow\}) \right] \times \det \left[ \phi_i^{k\downarrow}(\mathbf{r}_j^\downarrow; \{\mathbf{r}_{/j}^\downarrow\}; \{\mathbf{r}^\uparrow\}) \right] \quad (3)$$

where  $\omega_k$  is a variational parameter and orbitals  $\phi_i^{k\alpha}$  are constructed using artificial NNs.  $\{\mathbf{r}^\alpha\}$  is the set of all electrons positions with spin  $\alpha$ , and  $\{\mathbf{r}_{/j}^\alpha\}$  is the set of all electron positions with spin  $\alpha$  except the electron  $\mathbf{r}_j^\alpha$ . By construction, these orbitals are invariant under permutations of particles that are not the  $j$ -th particle. Furthermore, the determinant form ensures the global wave function is anti-symmetric.

The orbitals  $\phi_i^{k\alpha}$  are given by

$$\phi_i^{k\alpha}(\mathbf{r}_j^\alpha; \{\mathbf{r}_{/j}^\alpha\}; \{\mathbf{r}^{\bar{\alpha}}\}) = (\mathbf{w}_i^{k\alpha} \cdot \mathbf{h}_j^{L\alpha} + g_i^{k\alpha}) \pi_i^{k\alpha} \exp(-|\Sigma_i^{k\alpha} \mathbf{r}_j^\alpha|), \quad (4)$$

where  $\mathbf{w}_i^{k\alpha}$ ,  $g_i^{k\alpha}$ ,  $\pi_i^{k\alpha}$ , and  $\Sigma_i^{k\alpha}$  are variational parameters and  $\mathbf{h}_j^{L\alpha}$  are the NN outputs. The Kronecker-factored approximate curvature (KFAC) algorithm [35] is used to optimize the variational parameters of the trial wave function.

Besides the variational parameters, several hyperparameters are used to control various aspects of the NN architecture. Here, four primary hyperparameters are

considered. The first is the total number of layers, denoted by  $L$ , which determines the depth of the network. Two streams are constructed to manage the data flow: the one-electron stream  $\mathbf{h}_i^{\ell\alpha}$ , which processes inputs related to single-electron configurations, and the two-electron stream  $\mathbf{h}_{ij}^{\ell\alpha\alpha'}$ , which handles inputs related to two-electron configurations. Both streams are characterized by their respective widths, referring to the number of units in each layer. The last hyperparameter is the number of multi-orbital expansions, representing the number of linear combinations of determinants (maximum value of  $k$  in Eq. (3)).

The input of each stream considers information from the electron positions and their relative coordinates

$$\mathbf{h}_i^{0\alpha} = (\mathbf{r}_i^\alpha, |\mathbf{r}_i^\alpha|); \quad \mathbf{h}_{ij}^{0\alpha\alpha'} = (\mathbf{r}_i^\alpha - \mathbf{r}_j^{\alpha'}, |\mathbf{r}_i^\alpha - \mathbf{r}_j^{\alpha'}|). \quad (5)$$

Information on each stream flows from layers  $\ell$  to  $\ell + 1$  according to the expressions

$$\mathbf{h}_i^{\ell+1\alpha} = \tanh(\mathbf{V}^\ell \mathbf{f}_i^{\ell\alpha} + \mathbf{b}^\ell) + \mathbf{h}_i^{\ell\alpha}, \quad (6a)$$

$$\mathbf{h}_{ij}^{\ell+1\alpha\alpha'} = \tanh(\mathbf{W}^\ell \mathbf{h}_{ij}^{\ell\alpha\alpha'} + \mathbf{c}^\ell) + \mathbf{h}_{ij}^{\ell\alpha\alpha'}, \quad (6b)$$

where  $\mathbf{V}^\ell$  and  $\mathbf{W}^\ell$  are the weight matrices, while  $\mathbf{b}^\ell$  and  $\mathbf{c}^\ell$  are biases and  $\mathbf{f}_i^{\ell\alpha}$  are intermediate vectors

$$\mathbf{f}_i^{\ell\alpha} = \left( \mathbf{h}_i^{\ell\alpha}, \frac{1}{n^\uparrow} \sum_{j=1}^{n^\uparrow} \mathbf{h}_j^{\ell\uparrow}, \frac{1}{n^\downarrow} \sum_{j=1}^{n^\downarrow} \mathbf{h}_j^{\ell\downarrow}, \frac{1}{n^\uparrow} \sum_{j=1}^{n^\uparrow} \mathbf{h}_{ij}^{\ell\alpha\uparrow}, \frac{1}{n^\downarrow} \sum_{j=1}^{n^\downarrow} \mathbf{h}_{ij}^{\ell\alpha\downarrow} \right). \quad (7)$$

When optimizing a wave function for quantum systems using Monte Carlo methods, it is essential to account for both the statistical uncertainty arising from parameter variations and the inherent stochastic nature of the algorithm. These factors together lead to a distribution of energy values. Therefore, accurately characterizing quantum systems and their energy states during the optimization process requires careful consideration of both sources of variability to ensure reliable outcomes.

*Results* - We investigated the effectiveness of using machine learning, specifically neural networks, in representing wave functions for this fermionic system. Our focus was on QDs with up to 30 electrons, and we compared the results of our neural network-based variational Monte Carlo (NN-VMC) approach with the diffusion Monte Carlo (DMC) method using the fixed-node approximation.

The evolution of the total variational energy for a QD with 12 electrons during the optimization process is shown in Fig. 1. The variational energy initially decreases rapidly, followed by a more gradual decline. After

approximately 200,000 optimization steps, we observe energies below the DMC results that continue to decrease slowly with more iterations. The final variational energy obtained using our method is significantly lower than that achieved with the DMC fixed-node approximation (approximately 0.5%). This improvement is statistically significant, as the energy uncertainties are much smaller than this difference. Typical hyperparameter values for  $N = 12$  are 4 neural network layers, a width of 128 for the one-electron stream, 32 for the two-electron stream, and 8 determinants in the multi-orbital expansion.

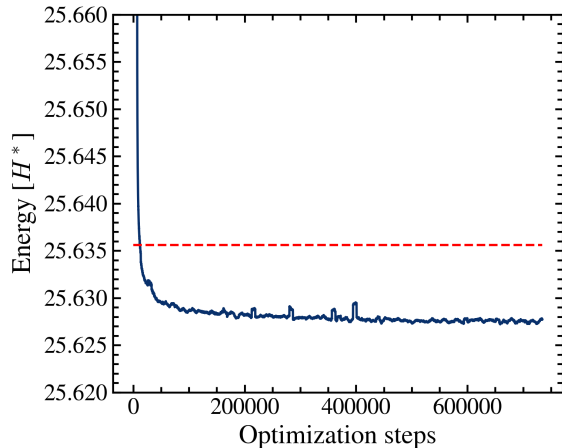


FIG. 1. Evolution of the variational total energy of a QD with 12 electrons in the NN-VMC algorithm. The dashed red line stands for a DMC result using the fixed-node approximation [36].

After the optimization process, we select the optimized set of variational parameters and perform a standard Monte Carlo integration to reduce statistical uncertainties further. The total energy results for QDs with 6, 12, 20, and 30 electrons, comparing our method with DMC and  $\Lambda$ -coupled-cluster singles-doubles (CCSD) [36], path-integral Monte Carlo (PIMC) [37], and in-medium similarity renormalization group (IM-SRG) [38] results are shown in Table I. Across all electron counts, our approach consistently yields lower energy values, except when comparing with IM-SRG for a few electrons. For example, for the 30-electron system, the total energy calculated using our neural network approach is  $123.9469(2) E_H^*$ , compared to  $123.9683(2) E_H^*$  from DMC, representing an improvement of  $0.02 E_H^*$ . It is important to note that, due to operator truncations, the IM-SRG method might produce energy results that violate the variational principle (energies lower than the true ground state energy).

To evaluate the nodal structures generated by our neural network representation, we compared the wave function with a harmonic oscillator trial function—the usual Slater determinant of non-interacting harmonic oscillator orbitals with the harmonic frequency as a variational

TABLE I. Total energies for QDs with 6, 12, 20, and 30 electrons in units of  $E_H^*$ . The first row shows the number of electrons in the QD. The second row are results obtained in this work. The third, fourth, fifth, and sixth rows are results from DMC, PIMC, CCSD, and IM-SRG calculations, respectively, from a collection of references (<sup>a</sup>[36], <sup>b</sup>[37], <sup>c</sup>[39], <sup>d</sup>[38]).

N	6	12	20	30
This work	7.59703(9)	25.62599(6)	61.9073(1)	123.9372(1)
DMC	7.6001(1) <sup>a</sup>	25.6356(1) <sup>a</sup>	61.922(2) <sup>a</sup>	123.9683(2) <sup>c</sup>
PIMC	7.5980(1) <sup>b</sup>	25.6456(6) <sup>b</sup>	61.992(3) <sup>b</sup>	N/A
CCSD	7.6044 <sup>a</sup>	25.6439 <sup>a</sup>	61.9375 <sup>a</sup>	124.3630 <sup>d</sup>
IM-SRG	7.5731 <sup>d</sup>	25.6259 <sup>d</sup>	61.9585 <sup>d</sup>	124.1041 <sup>d</sup>

parameter. Fig. 2 shows a two-dimensional color map of the hyperplane of our optimized trial function for a QD with 20 electrons, with the white lines indicating the nodal surfaces. The figure was constructed by selecting an equilibrated configuration from our trial function and fixing all electron coordinates but one (red arrow), which was then moved over the QD. The wave function values are shown in the color scale, with the numerical axis representing the coordinates of the moving electron. The same initial configuration was used for the non-NN wave function with the optimal variational parameter.

The nodal regions of the neural network-derived hyperplanes in blue (right) are smoother and exhibit less curvature compared to the traditional trial function represented in green (left), leading to a reduction in kinetic energy and an overall more accurate representation of the system. The comparison was repeated by choosing different initial electronic configurations, also including electrons with spin down. The result was always consistent with the one we show in Fig. 2. Naturally, changing the electron being moved impacts the overall aspect of the corresponding nodal structure (see figures in the supplemental material).

Showcasing the ability of the neural-network wave function to yield accurate results for physical properties of the system, in Fig. 3 we show results for radial distribution functions of different relative electronic spin orientations. Furthermore, the two dimensional density profile for a QD can be computed through

$$\eta_{2D}(\mathbf{r}) = \sum_i \delta(\mathbf{r}_i - \mathbf{r}), \quad (8)$$

normalized by imposing  $\int \eta_{2D}(\mathbf{r}) dA = 1$ . The result for a QD with 20 electrons is displayed in Fig. 4. Although the circular symmetry was not explicitly imposed, our neural network was able to capture this feature during training. This reinforces the flexibility and effectiveness of our approach in representing complex wave functions without prior assumptions about the geometry of the system.

The energy uncertainties in our results are small,

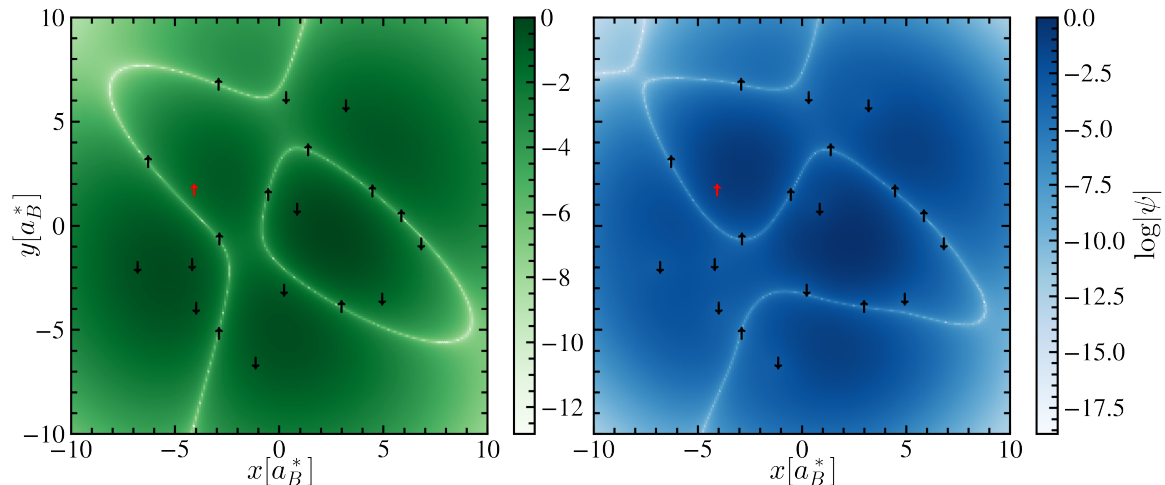


FIG. 2. Nodal structure of trial functions of a QD with  $N = 20$  electrons. (Left) A trial function of the harmonic oscillator form. (Right) Neural network representation of the ML-learned wave function. Up (down) arrows stand for up (down) spins. The red arrow depicts the electron that is moved over the hyperplane, all others being fixed.

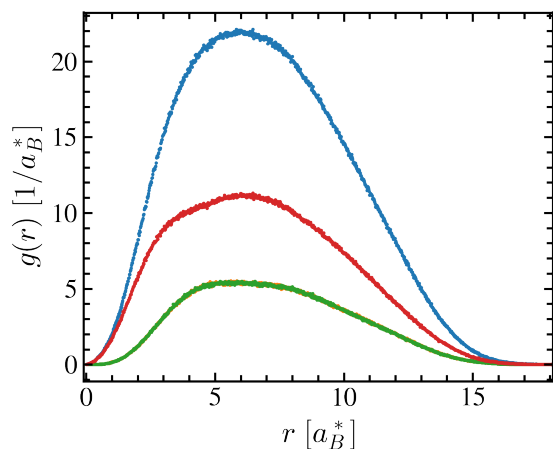


FIG. 3. Pair distribution functions in units of  $1/a_0^*$ , the inverse of the effective Bohr radius, as a function of the electrons separation. The pair distribution functions for up-up spins and down-down spins are collapsed in the figure scale, they are visible in green. In red is depicted  $g_{\uparrow\downarrow}(r)$  and in blue  $g(r)$  of the electrons regardless their spin.

demonstrating the robustness of the simulations. For instance, the standard deviation in the energy of the 12-electron system is only  $0.00009 E_H^*$ , indicating the statistical significance of the observed improvements over the DMC method. These results confirm that our machine learning-based approach can reliably reduce the variational bias in quantum Monte Carlo simulations.

*Conclusion* - Several sophisticated approaches have been proposed to mitigate or circumvent the sign problem in QMC simulations of Fermi systems [40–44]. The

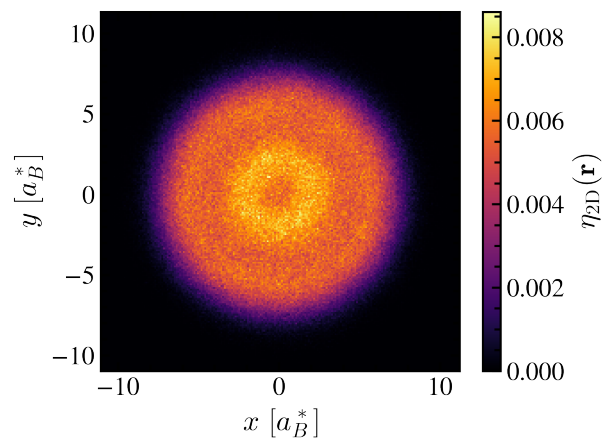


FIG. 4. A normalized bi-dimensional histogram of the electronic positions of a QD of 20 electrons.

fixed-node approximation is a popular approach and has yielded results for various systems [36, 39, 45–51], but introduces an intrinsic bias through an *a priori* chosen nodal structure.

Our work demonstrates that machine learning, specifically neural network-based representations of wave functions, offers a promising solution to these longstanding challenges. By leveraging deep neural networks, we were able to construct more accurate nodal structures for quantum dots systems and reduce the variational bias introduced in QMC simulations. For QDs with up to 30 electrons, our method resulted in statistically superior values to those obtained through the traditional diffusion Monte Carlo with the fixed-node approximation.

This work not only confirms the feasibility of using machine learning to overcome the limitations of conventional QMC methods but also highlights its potential for widespread application in strongly correlated many-body systems. Our approach represents a significant step forward in quantum simulations, offering a flexible and powerful tool for improving the accuracy of predictions in complex quantum systems.

Moreover, integrating machine learning techniques with quantum simulations holds great promise for advancing quantum technologies, such as scalable quantum computing and materials discovery. Future research should focus on refining neural network architectures to handle larger quantum systems. ML approaches can largely benefit from GPU acceleration and the easiness of algorithm implementation coming from a very rich ecosystem of software packages and libraries (PyTorch, TensorFlow, JAX, and others), making downstream tasks that depend on the system's wave function and its derivatives an efficient possibility.

*Acknowledgements* - SAV acknowledges financial support from the Brazilian agency, Fundação de Amparo à Pesquisa do Estado de São Paulo grant #2023/07225-0, São Paulo Research Foundation (FAPESP). WF acknowledges financial support also from FAPESP, grant #2020/10505-6. This work used Delta at the National Center for Supercomputing Applications through allocation CIS230072 from the Advanced Cyberinfrastructure Coordination Ecosystem: Services & Support (ACCESS) program, which is supported by U.S. National Science Foundation grants #2138259, #2138286, #2138307, #2137603, and #2138296 [52].

- 
- [1] S. Paschen and Q. Si, Quantum phases driven by strong correlations, *Nature Reviews Physics* **3**, 9 (2020).
- [2] S. Adler, F. Krien, P. Chalupa-Gantner, G. Sangiovanni, and A. Toschi, Non-perturbative intertwining between spin and charge correlations: A “smoking gun” single-boson-exchange result, *SciPost Physics* **16**, 054 (2024).
- [3] D. R. Baykusheva, M. H. Kalthoff, D. Hofmann, M. Claassen, D. M. Kennes, M. A. Sentef, and M. Mitra, Witnessing Nonequilibrium Entanglement Dynamics in a Strongly Correlated Fermionic Chain, *Physical Review Letters* **130**, 106902 (2023).
- [4] J. Carlström, Strong-coupling diagrammatic Monte Carlo technique for correlated fermions and frustrated spins, *Physical Review B* **103**, 195147 (2021).
- [5] J. Bloch, A. Cavalleri, V. Galitski, M. Hafezi, and A. Rubio, Strongly correlated electron photon systems, *Nature* **606**, 41 (2022).
- [6] L. K. Wagner and D. M. Ceperley, Discovering correlated fermions using quantum Monte Carlo, *Reports on Progress in Physics* **79**, 094501 (2016).
- [7] Z. Lv, Y. Wang, J. Chen, J. Wang, Y. Zhou, and S.-T. Han, Semiconductor Quantum Dots for Memories and Neuromorphic Computing Systems, *Chemical Reviews* **120**, 3941 (2020).
- [8] N. P. De Leon, K. M. Itoh, D. Kim, K. K. Mehta, T. E. Northup, H. Paik, B. S. Palmer, N. Samarth, S. Sangtawesin, and D. W. Steuerman, Materials challenges and opportunities for quantum computing hardware, *Science* **372**, eabb2823 (2021).
- [9] R. Uppu, L. Midolo, X. Zhou, J. Carolan, and P. Lodahl, Quantum-dot-based deterministic photon emitter interfaces for scalable photonic quantum technology, *Nature Nanotechnology* **16**, 1308 (2021).
- [10] C. Sikorski and U. Merkt, Spectroscopy of electronic states in insb quantum dots, *Physical Review Letters* **62**, 2164 (1989-05).
- [11] P. A. Maksym and T. Chakraborty, Quantum dots in a magnetic field: Role of electron-electron interactions, *Physical Review Letters* **65**, 108 (1990-07).
- [12] T.-K. Hsiao, P. Cova Fariña, S. D. Oosterhout, D. Jirovec, X. Zhang, C. J. van Diepen, W. I. L. Lawrie, C.-A. Wang, A. Sammak, G. Scappucci, M. Veldhorst, E. Demler, and L. M. K. Vandersypen, Exciton transport in a germanium quantum dot ladder, *Physical Review X* **14**, 011048 (2024-03).
- [13] D. Degli Esposti, L. E. A. Stehouwer, Ö Gül, N. Samkharadze, C. Déprez, M. Meyer, I. N. Meijer, L. Tryputen, S. Karwal, M. Botifoll, J. Arbiol, S. V. Amitonov, L. M. K. Vandersypen, A. Sammak, M. Veldhorst, and G. Scappucci, Low disorder and high valley splitting in silicon, *npj Quantum Information* **10**, 10.1038/s41534-024-00826-9 (2024-03).
- [14] V. John, F. Borsoi, Z. György, C.-A. Wang, G. Széchenyi, F. van Riggelen-Doelman, W. I. L. Lawrie, N. W. Hendrickx, A. Sammak, G. Scappucci, A. Pályi, and M. Veldhorst, Bichromatic rabi control of semiconductor qubits, *Physical Review Letters* **132**, 067001 (2024-02).
- [15] M. Meyer, C. Déprez, I. N. Meijer, F. K. Unseld, S. Karwal, A. Sammak, G. Scappucci, L. M. K. Vandersypen, and M. Veldhorst, Single-electron occupation in quantum dot arrays at selectable plunger gate voltage, *Nano Letters* **23**, 11593 (2023-12).
- [16] F. Borsoi and M. Veldhorst, A tunable two-dimensional crossbar array comprising 16 quantum dots, *Nature Nanotechnology* **19**, 7 (2023-09).
- [17] F. Borsoi, N. W. Hendrickx, V. John, M. Meyer, S. Motz, F. van Riggelen, A. Sammak, S. L. de Snoo, G. Scappucci, and M. Veldhorst, Shared control of a 16 semiconductor quantum dot crossbar array, *Nature Nanotechnology* **19**, 21 (2023-08).
- [18] W. I. L. Lawrie, M. Rimbach-Russ, F. v. Riggelen, N. W. Hendrickx, S. L. d. Snoo, A. Sammak, G. Scappucci, J. Helsen, and M. Veldhorst, Simultaneous single-qubit driving of semiconductor spin qubits at the fault-tolerant threshold, *Nature Communications* **14**, 10.1038/s41467-023-39334-3 (2023-06).
- [19] X. Wang, E. Khatami, F. Fei, J. Wyrick, P. Namboodiri, R. Kashid, A. F. Rigosi, G. Bryant, and R. Silver, Experimental realization of an extended Fermi-Hubbard model using a 2D lattice of dopant-based quantum dots, *Nature Communications* **13**, 6824 (2022).
- [20] M. Kiczynski, S. K. Gorman, H. Geng, M. B. Donnelly, Y. Chung, Y. He, J. G. Keizer, and M. Y. Simmons, Engineering topological states in atom-based semiconductor quantum dots, *Nature* **606**, 694 (2022).
- [21] M. Iazzi, A. A. Soluyanov, and M. Troyer, Topological

- origin of the fermion sign problem, *Physical Review B* **93**, 115102 (2016).
- [22] R. Mondaini, S. Tarat, and R. T. Scalettar, Universality and critical exponents of the fermion sign problem, *Physical Review B* **107**, 245144 (2023).
- [23] A. C. Cosentini, M. Capone, L. Guidoni, and G. B. Bachelet, Phase separation in the two-dimensional Hubbard model: A fixed-node quantum Monte Carlo study, *Physical Review B* **58**, R14685 (1998).
- [24] J. Yu, L. K. Wagner, and E. Ertekin, Fixed-node diffusion Monte Carlo description of nitrogen defects in zinc oxide, *Physical Review B* **95**, 075209 (2017).
- [25] K. M. Rasch and L. Mitas, Fixed-node diffusion Monte Carlo method for lithium systems, *Physical Review B* **92**, 045122 (2015).
- [26] R. Nazarov, L. Shulenburger, M. Morales, and R. Q. Hood, Benchmarking the pseudopotential and fixed-node approximations in diffusion Monte Carlo calculations of molecules and solids, *Physical Review B* **93**, 094111 (2016).
- [27] S. Johnston, E. Khatami, and R. Scalettar, A perspective on machine learning and data science for strongly correlated electron problems, *Carbon Trends* **9**, 100231 (2022).
- [28] P.-L. Zheng, J.-B. Wang, and Y. Zhang, Efficient and quantum-adaptive machine learning with fermion neural networks, *Physical Review Applied* **20**, 044002 (2023).
- [29] W. T. Lou, H. Sutterud, G. Cassella, W. Foulkes, J. Knolle, D. Pfau, and J. S. Spencer, Neural Wave Functions for Superfluids, *Physical Review X* **14**, 021030 (2024).
- [30] A. Harju, Variational monte carlo for interacting electrons in quantum dots, *Journal of Low Temperature Physics* **140**, 181 (2005-07).
- [31] F. Pederiva, C. J. Umrigar, and E. Lipparini, Diffusion Monte Carlo study of circular quantum dots, *Physical Review B* **62**, 8120 (2000).
- [32] D. P. James S. Spencer and F. Contributors, FermiNet, <http://github.com/deepmind/ferminet> (2020).
- [33] W. Freitas and S. A. Vitiello, Synergy between deep neural networks and the variational Monte Carlo method for small  ${}^4\text{He}_n$  clusters, *Quantum* **7**, 1209 (2023-12), <https://quantum-journal.org/papers/q-2023-12-18-1209/>.
- [34] W. Freitas, B. Abreu, and S. A. Vitiello, Modeling  ${}^4\text{He}_N$  clusters with wave functions based on neural networks, *Journal of Low Temperature Physics* 10.1007/s10909-024-03061-w (2024-03).
- [35] J. Martens and R. B. Grosse, Optimizing neural networks with kronecker-factored approximate curvature, in *ICML'15: Proceedings of the 32nd International Conference on International Conference on Machine Learning - Volume 37* (2015).
- [36] M. P. Lohne, G. Hagen, M. Hjorth-Jensen, S. Kvaal, and F. Pederiva, Ab initio computation of the energies of circular quantum dots, *Physical Review B* **84**, 10.1103/physrevb.84.115302 (2011).
- [37] I. Kylänpää and E. Räsänen, Path integral monte carlo benchmarks for two-dimensional quantum dots, *Phys. Rev. B* **96**, 205445 (2017).
- [38] F. Yuan, S. J. Novario, N. M. Parzuchowski, S. Reimann, S. K. Bogner, and M. Hjorth-Jensen, Addition and removal energies of circular quantum dots, *The Journal of Chemical Physics* **147**, 164109 (2017).
- [39] J. Høgberget, *Quantum Monte-Carlo studies of generalized many-body systems*, Master's thesis, Faculty of Mathematics and Natural Sciences, Department of Physics, University of Oslo (2013).
- [40] M. Ulybyshev, C. Winterowd, and S. Zafeiropoulos, Lefschetz thimbles decomposition for the hubbard model on the hexagonal lattice, *Physical Review D* **101**, 014508 (2020-01).
- [41] M. Körner, K. Langfeld, D. Smith, and L. von Smekal, Density of states approach to the hexagonal hubbard model at finite density, *Physical Review D* **102**, 054502 (2020-09).
- [42] R. Levy and B. K. Clark, Mitigating the sign problem through basis rotations, *Physical Review Letters* **126**, 216401 (2021-05).
- [43] Z. Wei, C. Wu, Y. Li, S. Zhang, and T. Xiang, Majorana positivity and the fermion sign problem of quantum monte carlo simulations, *Physical Review Letters* **116**, 250601 (2016-06).
- [44] J. S. Hofmann, E. Khalaf, A. Vishwanath, E. Berg, and J. Y. Lee, Fermionic monte carlo study of a realistic model of twisted bilayer graphene, *Physical Review X* **12**, 011061 (2022-03).
- [45] T. A. Anderson, M. C. Per, and C. J. Umrigar, Reducing the time-step errors in diffusion monte carlo, *The Journal of Chemical Physics* **160**, 10.1063/5.0190346 (2024-03).
- [46] R. Pessoa, S. A. Vitiello, and L. A. P. Ardila, Fermi polaron in atom-ion hybrid systems, *ArXiv e-prints* 10.48550/ARXIV.2401.05324 (2024).
- [47] R. Curry, J. E. Lynn, K. E. Schmidt, and A. Gezerlis, Second-order perturbation theory in continuum quantum monte carlo calculations, *Physical Review Research* **5**, 1042021 (2023-11).
- [48] S. Shepard, R. L. Panadés-Barrueta, S. Moroni, A. Scemama, and C. Filippi, Double excitation energies from quantum monte carlo using state-specific energy optimization, *Journal of Chemical Theory and Computation* **18**, 6722 (2022-10).
- [49] J. van Rhijn, C. Filippi, S. De Palo, and S. Moroni, Energy derivatives in real-space diffusion monte carlo, *Journal of Chemical Theory and Computation* **18**, 118 (2021-12).
- [50] T. Frank, R. Derian, K. Tokár, L. Mitas, J. Fabian, and I. Åtich, Many-body quantum monte carlo study of 2d materials: Cohesion and band gap in single-layer phosphorene, *Physical Review X* **9**, 011018 (2019-01).
- [51] M. Ditte and M. Dubecky, Fractional charge by fixed-node diffusion monte carlo method, *Physical Review Letters* **123**, 156402 (2019-10).
- [52] T. J. Boerner, S. Deems, T. R. Furlani, S. L. Knuth, and J. Towns, ACCESS: Advancing Innovation: NSF's Advanced Cyberinfrastructure Coordination Ecosystem: Services & Support, in *Practice and Experience in Advanced Research Computing* (ACM, Portland OR USA, 2023) pp. 173–176.

Supplementary materials for

## **Machine-learned nodal structures of Fermion systems**

William Freitas,<sup>1</sup> Bruno Abreu,<sup>2</sup> and S. A. Vitiello<sup>1</sup>

<sup>1</sup>*Gleb Wataghin Institute of Physics,  
University of Campinas (UNICAMP), 13083-970 Campinas, SP, Brazil*

<sup>2</sup>*Pittsburgh Supercomputing Center,  
Carnegie Mellon University, Pittsburgh, PA 15213, USA*

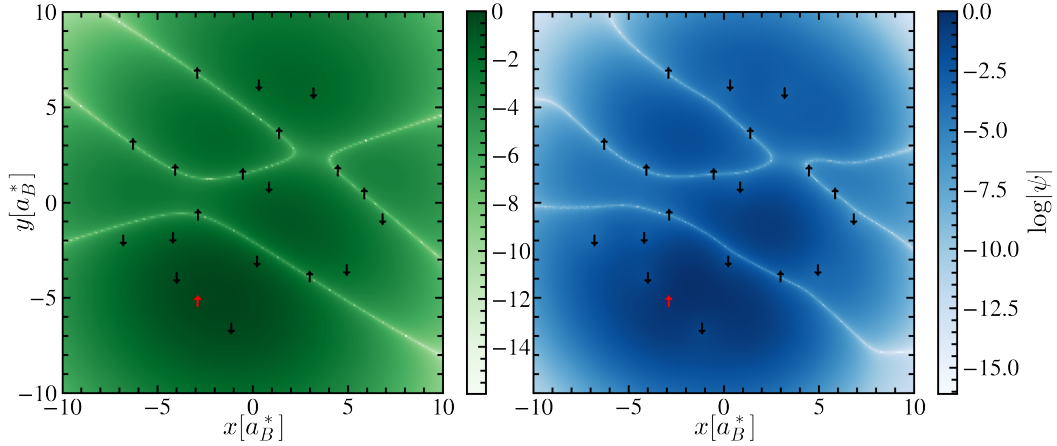


FIG. 1. Configuration 1, electron 2 (red). Nodal structure of trial functions of a QD with  $N = 20$  electrons. (Left) A trial function of the harmonic oscillator form. (Right) Neural network representation of the ML-learned wave function. Up (down) arrows stand for up (down) spins. The red arrow depicts the electron that is moved over the hyperplane, all others being fixed.

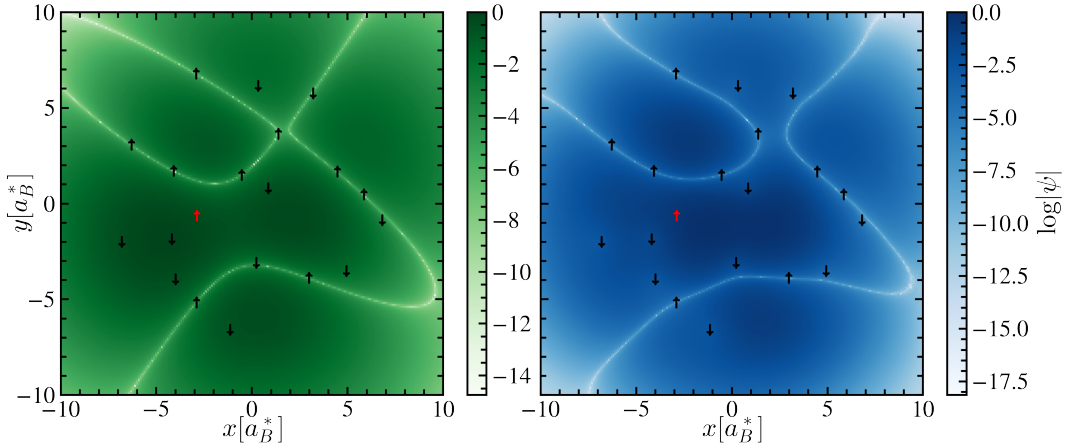


FIG. 2. Configuration 1, electron 3 (red). Nodal structure of trial functions of a QD with  $N = 20$  electrons. (Left) A trial function of the harmonic oscillator form. (Right) Neural network representation of the ML-learned wave function. Up (down) arrows stand for up (down) spins. The red arrow depicts the electron that is moved over the hyperplane, all others being fixed.



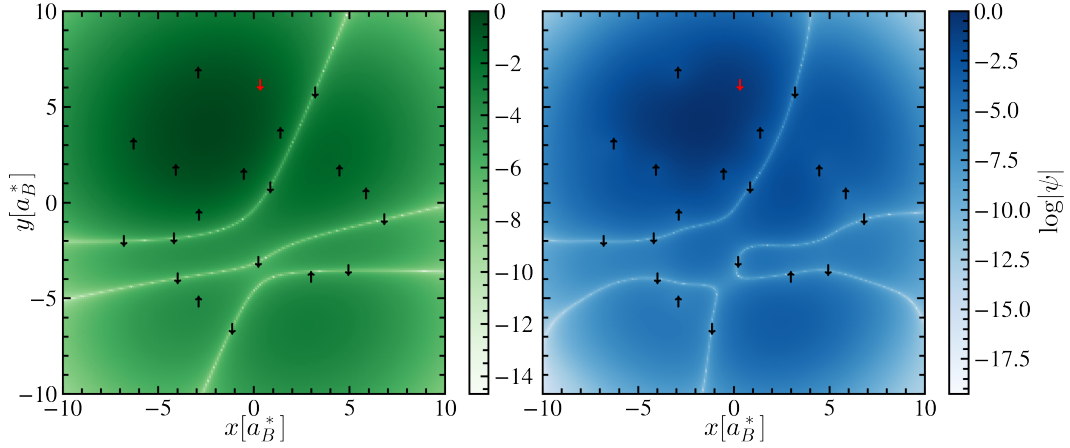


FIG. 3. Configuration 1, electron 11 (red). Nodal structure of trial functions of a QD with  $N = 20$  electrons. (Left) A trial function of the harmonic oscillator form. (Right) Neural network representation of the ML-learned wave function. Up (down) arrows stand for up (down) spins. The red arrow depicts the electron that is moved over the hyperplane, all others being fixed.

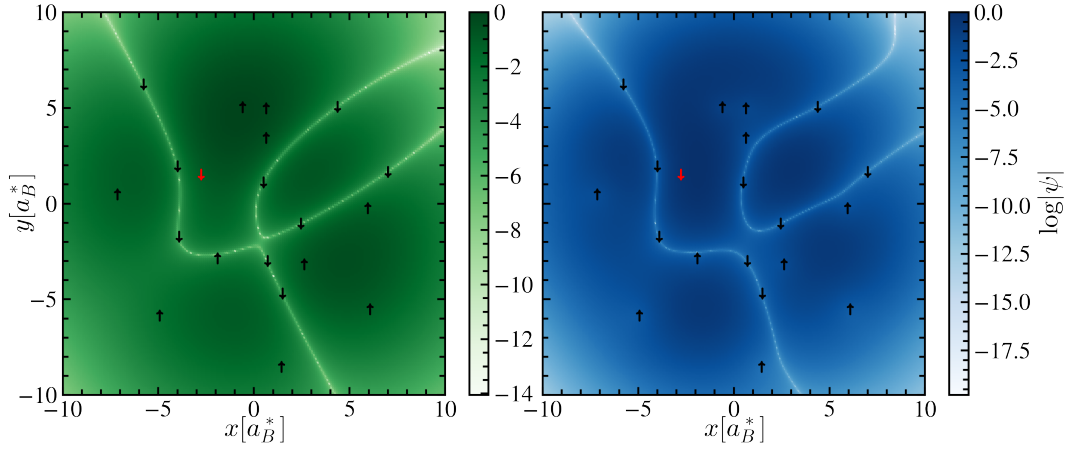


FIG. 4. Configuration 2, electron 11 (red). Nodal structure of trial functions of a QD with  $N = 20$  electrons. (Left) A trial function of the harmonic oscillator form. (Right) Neural network representation of the ML-learned wave function. Up (down) arrows stand for up (down) spins. The red arrow depicts the electron that is moved over the hyperplane, all others being fixed.

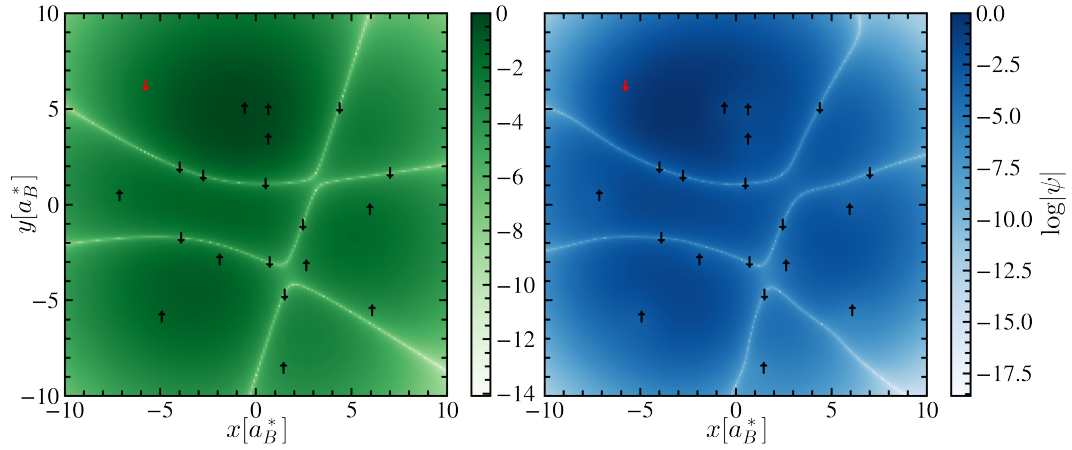


FIG. 5. Configuration 2, electron 12 (red). Nodal structure of trial functions of a QD with  $N = 20$  electrons. (Left) A trial function of the harmonic oscillator form. (Right) Neural network representation of the ML-learned wave function. Up (down) arrows stand for up (down) spins. The red arrow depicts the electron that is moved over the hyperplane, all others being fixed.